ELSEVIER

Journal of Alloys and Compounds 330–332 (2002) 871–874

Journal of ALLOYS AND COMPOUNDS

www.elsevier.com/locate/jallcom

# Effect of the cooling rate of superstoichiometric $AB_5$ alloys with low Co content on their electrochemical performances

C. Audry[a], P. Bernard[a], Y. Champion[b], B. Knosp[a,*], L. Mazerolles[b], P. Ochin[b]

[a]*SAFT, Direction de la Recherche, 111 bd Alfred Daney, 33074 Bordeaux Cedex, France*
[b]*CECM, 15 rue Georges Urbain, 94407 Vitry sur Seine, France*

**Abstract**

Effects of cooling rate on microstructure and electrochemical performances of superstoichiometric $AB_5$ alloys with 5 wt.% Co have been investigated. Flakes of thickness ranging from 30 to 100 μm were obtained by melt spinning. The alloy microstructure was characterised using X-ray diffraction (XRD), scanning electron microscopy (SEM), transmission electron microscopy (TEM) and energy dispersive X-ray (EDX) microanalysis. Electrochemical evaluation did not show significant effect of the cooling rate on the initial capacity, but a noticeable effect was observed on cycle life and on corrosion rate after cycling. These results are discussed in terms of microstructural observations. 

*Keywords:* $AB_5$; Melt spinning; TEM; Electrode; Cycle stability; Corrosion

## 1. Introduction

Ni–MH batteries made of $AB_5$ alloy containing mischmetal (Mm), Ni, Mn, Al and 10 wt.% Co as a negative electrode material are now widely used in portable or electric vehicles (EV). Their performances in terms of capacity and cycle life are satisfactory but for mass market like EV applications, the cost must be reduced. In the negative electrode, an important way of cost reduction is to decrease the Co content in the alloy. However, it is well known that the decrease of Co content is detrimental in terms of battery cycle life [1]. Indeed, lowering the Co content induces an increase of the alloy corrosion, mainly due to an enhanced alloy decrepitation (fracture of the alloy upon hydriding dehydriding cycles). An alternative for reducing decrepitation of $AB_5$ alloys is to increase the stoichiometric ratio B/A [2–5]. Besides, a beneficial effect, in terms of corrosion resistance, of $AB_5$ alloys prepared by rapid cooling process has been already reported [5–9].

The objective of this work is to study the effect of the cooling rate on the microstructure and electrochemical performances of superstoichiometric low cost alloys containing about 5 wt.% Co.

## 2. Experimental

### 2.1. Preparation and characterisation of alloys

Ingots (800 g) containing about 5 wt.% Co were prepared by r.f. induction melting and casting under argon atmosphere. Then ingot lumps of 50 g were remelted and quenched to flakes, on a Cu–(Co–Be) wheel, following the planar flow casting technique under argon atmosphere. The flake thickness and the related cooling rate depend essentially on the linear velocity of the wheel. Various conditions of casting, corresponding to different linear wheel velocities ranging from 6 to 20 m $s^{-1}$, were applied for obtaining flakes of different thickness. Main parameters and flake characteristics are reported in Table 1.

The average composition of samples, determined by inductively coupled plasma (ICP) spectroscopy was $Ml(Ni, Mn, Al)_{4.87}Co_{0.42}$ (stoichiometry=5.29 with 0.004 standard deviation), where Ml is a La-rich mischmetal with 10% Ce. No significant deviation from this composition was observed with respect to the melt spinning conditions.

Table 1
Preparation conditions and thickness of the studied alloys

| Alloy | A | B | C | D |
|---|---|---|---|---|
| Wheel linear velocity $V_L$ (m $s^{-1}$) | 6 | 9.8 | 15 | 19 |
| Thickness (μm) | 100 | 55 | 38 | 30 |

*Corresponding author.

0925-8388/02/$ – see front matter 
PII: S0925-8388(01)01653-X

Flake thickness was measured by optical microscopy of polished cross sections. The alloy microstructures were examined by scanning electron microscopy (SEM) using a JEOL JSM 6330 F microscope equipped with an energy dispersive X-ray (EDX) microprobe of size ~1 μm. Thin specimens were obtained from flakes by $Ar^+$ ion sputtering and were examined by transmission electron microscopy (TEM) using an AKASHI-TOPCON microscope (1.8 Å point resolution) with an EDX probe 20 nm in size. The alloy crystallographic structure was investigated by X-ray diffraction (XRD) using a Siemens D5000 diffractometer with Kα Cu anticathode.

### 2.2. Electrochemical evaluation

For electrochemical evaluation, alloys were pulverised by mechanical grinding and powders were sieved between 20 and 63 μm. Afterwards, negative electrodes were prepared with a mixture consisting of alloy powder, PTFE as a binder and Ni powder for electrical conductivity. Then negative limited vented cells were assembled in plastic cases with one negative electrode isolated by a polyolefine separator from two positive foam electrodes containing $Ni_{1-x-y}Co_xZn_y(OH)_2$ active material and Co compounds as conductive material. Finally, the cells were filled with a standard 8.7 M KOH aqueous solution as electrolyte. For each alloy five cells were tested.

After 10 cycles of activation, accelerated cycle tests were carried out at the C rate (300 mA $g^{-1}$) for 48 min in discharge (80% depth of discharge, DOD) and 52 min in charge (8% overcharge). Capacities were periodically measured using the following conditions: (i) 16 h charge at the C/10 rate (30 mA $g^{-1}$); (ii) discharge at the C/5 rate (60 mA $g^{-1}$), 0.9 V cut-off voltage.

After electrochemical evaluation, corrosion rates were measured by ICP analysis of Al eluted out of the alloy and trapped in the positive electrode [10,11]. Besides, cycled negative electrodes were examined by SEM in order to estimate alloy decrepitation.

## 3. Results

Four alloys (A to D) were obtained in the form of flakes with thickness ranging from 30 to 100 μm (Table 1), which correspond approximately to cooling rates between $10^5$ and $10^6$ K $s^{-1}$. It arises that flake thickness decreases when the linear velocity $V_L$ increases.

### 3.1. Microstructural characterisation

Lattice parameters of the alloys and the unit cell volumes (Table 2) were calculated from the XRD patterns, assuming a single hexagonal structure of the $CaCu_5$ type. The parameter *c* does not depend significantly on the flake thickness. But the alloy D, relating to the highest cooling rate, seems to exhibit a lower parameter *a*, and consequently a lower unit cell volume *V*, than the other alloys.

Table 2
Results of microstructural characterisation of the alloys

| Alloy | A | B | C | D |
|---|---|---|---|---|
| Thickness (μm) | 100 | 55 | 38 | 30 |
| *a* (Å) | 5.038 | 5.037 | 5.035 | 5.030 |
| *c* (Å) | 4.058 | 4.059 | 4.060 | 4.061 |
| *V* ($Å^3$) | 89.21 | 89.19 | 89.15 | 89.00 |
| *G* (μm) | 1–2.5 | 0.5–2 | 0.5–1.3 | 0.3–1 |

Lattice parameters of the $CaCu_5$ hexagonal phase and unit cell volume *V* from XRD. Grain sizes *G* from TEM examinations.

SEM examinations showed a single phase microstructure whatever the thickness. An EDX (1 μm probe) semi-quantitative line scan did not show any heterogeneity in terms of composition through the thickness of one 100-μm-thick flake of alloy A (Fig. 1a). However, variations of Ni and Mn contents were observed through one 200-μm-thick flake of the same alloy (Fig. 1b). Specimens of alloys B–D appeared homogeneous in terms of chemical composition within the spatial resolution of the EDX probe (20 nm) associated with TEM and no segregation was detected at the grain boundaries.

Typical microstructure of rapidly quenched alloys was observed by TEM. The grains are elongated and the grain boundaries exhibit non-equilibrium high curvatures. Grain size ranging from 2.5–1 μm to 1–0.3 μm is related to the quenching rate and then the fraction of intercrystalline regions (grain-boundaries and triple junction) increases sharply when the quenching rate increases. In addition, a significant amount of disordered plate-like extended defects were observed in sample D, referring to the specimen having the highest cooling rate. Besides, TEM revealed contrasts associated to lattice distortions and dislocations pile-up in all samples. However, the level of distortions and dislocation density increased with the flake thickness.

### 3.2. Electrochemical evaluation

Specific capacity variations (symbols) during cycling are compared with those of a standard 10 wt.% Co $AB_5$ alloy of composition $MmNi_{3.55}Mn_{0.4}Al_{0.3}Co_{0.75}$ (Mm = mischmetal with 48% Ce) in Fig. 2. A linear regression line has been drawn for each alloy. The intercept $Q_o$ and the slope *P*, interpreted as the initial specific capacity after activation and a measure of the capacity loss, are presented in Table 3. Fig. 2 and Table 3 show that the initial capacities were not significantly different from one another. On the contrary, the capacity losses ranged from 0.04 mAh $g^{-1}$ $cycle^{-1}$ for alloy C (38 μm) to 0.25 mAh $g^{-1}$ $cycle^{-1}$ for alloy A (100 μm thick). Comparatively, the 10 wt.% Co standard alloy loss was 0.054 mAh $g^{-1}$ $cycle^{-1}$. In fact, it can be considered that the cycle stability

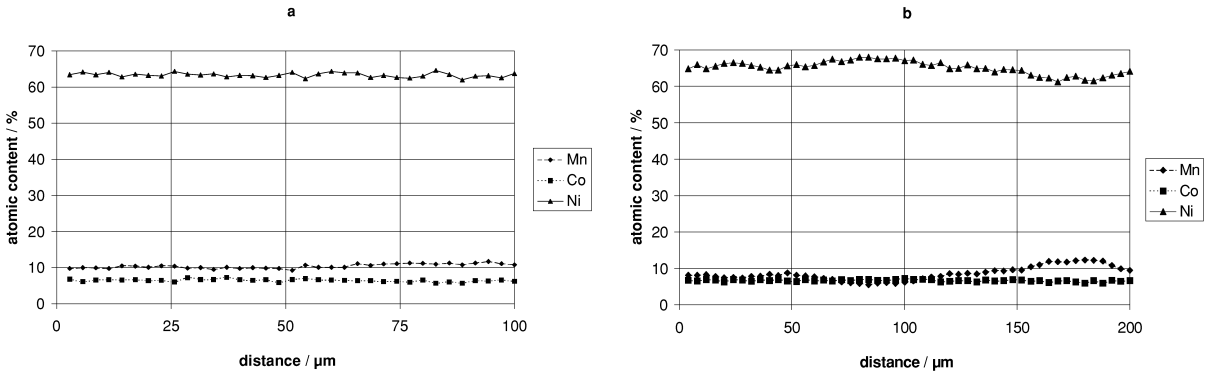


Fig. 1. Variations of Ni, Mn and Co contents in alloy A, as determined by semi-quantitative EDX line scan. (a) Through one 100-µm-thick flake, (b) through one 200-µm-thick flake.

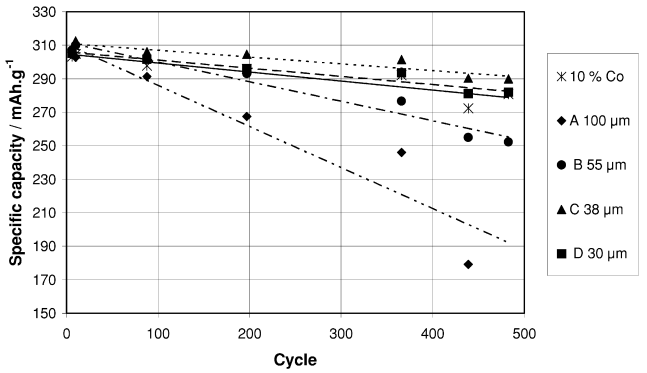


Fig. 2. Results of the electrochemical cycling at room temperature. (Cycling at the C rate, 80% DOD, 8% overcharge. Capacities measured at the 0.2 C discharge rate, 0.9 V cut-off voltage after 16 h charge at the 0.1 C rate).

of the superstoichiometric 5 wt.% Co alloys (A–D) increases when the flake thickness decreases (Fig. 3).

Corrosion rates at the end of the test (Table 3) increased from 8.9% for alloys C and D (thickness $<40$ µm) to 24.7% for alloy A (100 µm). Comparatively corrosion rate for the standard 10% Co alloy was 8.3%. These corrosion rates are well correlated with the capacity losses, as seen in Fig. 3. The corrosion rate behaviour as a function of the cooling rate can be explained because the level of decrepitation decreases when the thickness decreases (Fig. 4).

Table 3
Results of electrochemical tests and of corrosion measurements after cycling

| Alloy | A | B | C | D | 10% Co |
|---|---|---|---|---|---|
| Thickness (µm) | 100 | 55 | 38 | 30 | alloy |
| $Q_o$ (mAh g$^{-1}$) | 311 | 312 | 311 | 306 | 305 |
| $P \times 100$ (mAh g$^{-1}$ cycle$^{-1}$) | −24.6 | −11.7 | −4.1 | −4.9 | −5.4 |
| Corrosion rate (%) | 24.7 | 15.8 | 8.9 | 8.9 | 8.3 |

$Q_o$ is the intercept and $P$ is the slope of the regression line drawn in Fig. 2.

## 4. Discussion

Within the limit of the spatial resolution of the TEM EDX probe, local chemical variations may not be directly associated to the change in cycle life. In addition, an amorphous phase is unlikely to exist, because amorphous phase induces low capacities [8] and all the initial capacities are almost equal.

On the other hand, it is well known that the mechanical strength of an alloy increases as the inverse square root of the grain size (Hall Petch relationship). The limitation of this relationship has been discussed for very small grains [12], but seems to be valid for grains with size in the range of 150 nm and over [13]. The alloy grain size was reduced from 1–2.5 µm to 0.3–1 µm when the wheel velocity $V_L$ rose from 6 to 19 m s$^{-1}$. It can then be assumed that the mechanical strength of the studied alloys increases with the cooling rate.

TEM observations showed somehow, semi-quantitatively, that strains (and stresses) resulting from rapid cooling decreased when the cooling rate increased. This could be explained by an easier relaxation of stresses in intercrystalline regions, when the flake thickness decreases. So,

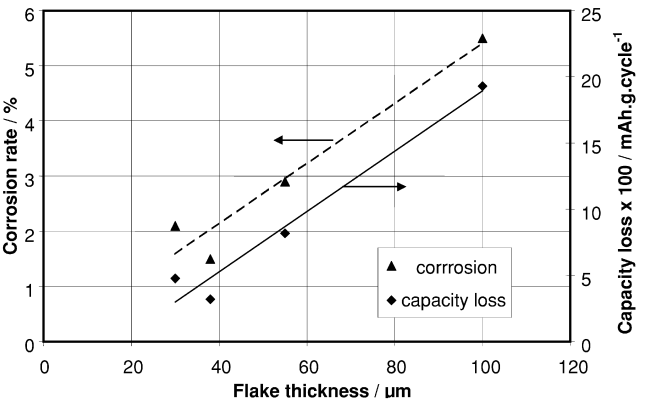


Fig. 3. Influence of the flake thickness on the corrosion rate and the capacity loss.

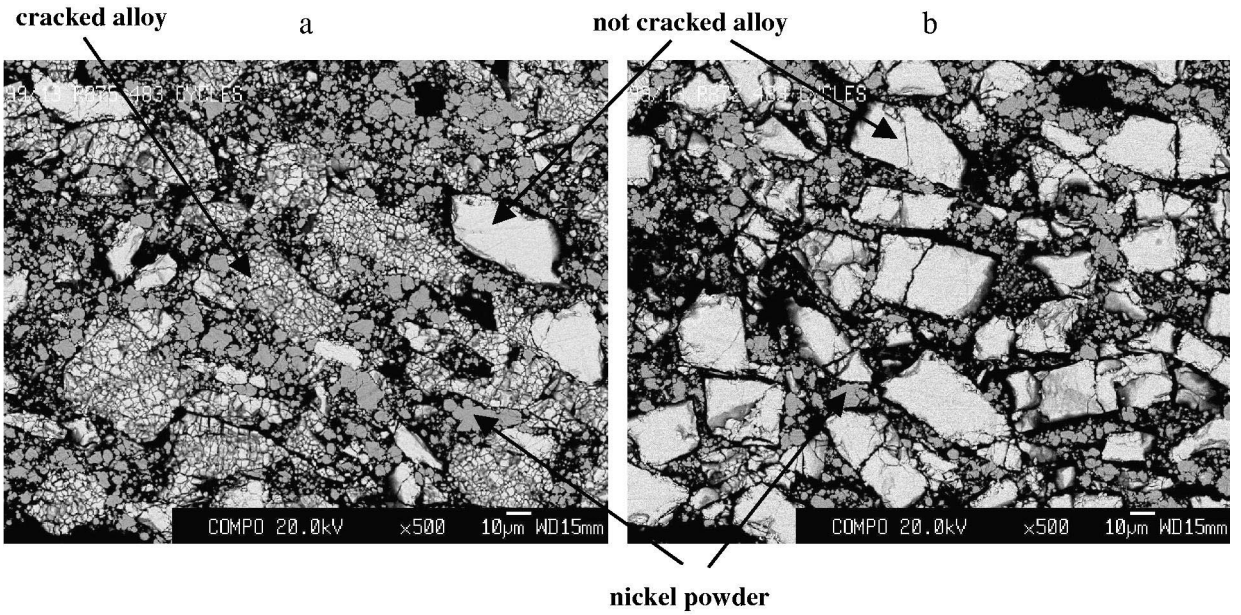


Fig. 4. SEM examination of alloy decrepitation after 483 electrochemical cycles. Grey areas consist of Ni powder added in electrodes. (a) Alloy A; (b) alloy D.

it can be assumed that the strain and stress level rise with the flake thickness.

In summary, we can assume that the alloy mechanical strength decreases and internal stresses increase when the flake thickness was augmented. If it is the case, more external stresses (due to hydrogen insertion for instance) would be necessary to reach the alloy strength of thinner flakes. This could explain, at least partly, the limited extent of decrepitation with higher cooling rates.

## 5. Conclusion

Alloys of superstoichiometric $AB_5$ composition containing 5 wt.% Co have been synthesised by melt spinning with different cooling rates as flakes of thickness ranging from 30 to 100 μm. Their microstructures were characterised by XRD, SEM and TEM associated with EDX microanalyses. Their electrochemical performances were evaluated in terms of capacity and cycle life.

Microstructural examinations did not show composition heterogeneity for flake thickness lower than 100 μm. But higher cooling rates led to smaller grain size (beneficial in terms of mechanical strength) and lower strain (or stress) levels.

The results of electrochemical tests showed that

- 5 wt.% Co superstoichiometric $AB_5$ alloys can be obtained with electrochemical performances comparable with those of standard 10 wt.% Co ones
- their capacity does not depend on the cooling rate
- high cooling rates are beneficial in terms of stability and corrosion resistance during cycling.

This beneficial effect in terms of cycle life results from a decreasing extent of decrepitation with increasing cooling rate. As the chemical composition appeared to be homogeneous in most cases, this reduction of decrepitation is attributed, at least partly, to an increase of the mechanical strength (due to the decreasing grain size) and/or to a decreasing level of strains (and stresses) when the cooling rate increases.

## References

[1] J.J.G. Willems, Philips J. Res. 39 (Suppl. 1) (1984) 1–94.
[2] P.H.L. Notten, R.E.F. Einerhand, J.L.C. Daams, J. Alloys Comp. 210 (1994) 221–232.
[3] J.M. Cocciantelli, P. Leblanc, G. Caillon, B. Knosp, Ph. Blanchard, J. Atkin, J. New Mater. Electrochem. Syst. 2 (1999) 151–155.
[4] P.H.L. Notten, M. Latroche, A. Percheron-Guégan, J. Electrochem. Soc 146 (1999) 3181–3189.
[5] P.H.L. Notten, J.L.C. Daams, R.E.F. Einerhand, Ber. Bunsenges Phys. Chem. 96 (1992) 656–667.
[6] N. Higashiyama, Y. Matsuura, H. Nakamura, M. Kimoto, M. Nogami, I. Yonezu, K. Nishio, J. Alloys Comp. 253–254 (1997) 648–651.
[7] H. Hasebe et al., European Patent Application 0 588 310 A2.
[8] C. Li, X. Wang, C. Wang, J. Alloys Comp. 266 (1998) 300–306.
[9] C.J. Li, X.L. Wang, J. Alloys Comp. 284 (1999) 270–273.
[10] P. Bernard, J. Electrochem. Soc. 145 (1998) 456–458.
[11] P. Leblanc, C. Jordy, B. Knosp, Ph. Blanchard, J. Electrochem. Soc. 145 (1998) 860–863.
[12] E. Artz, Acta Mater. 46 (1998) 5611–5626.
[13] R.W. Cahn, A.L. Greer, in: R.W. Cahn, P. Haasen (Eds.), 4th Edition, Physical Metallurgy, 1996, pp. 1815–1817, Chapter 19.